Chemical routes to materials

In situ synthesis of Fe_3O_4-reinforced carbon fiber composites as anodes in lithium-ion batteries

Mandana Akia[1], Nataly Salinas[1], Salomon Luna[1], Elizabeth Medina[1], Alejandra Valdez[1], Jorge Lopez[1], Jonathan Ayala[1], Mataz Alcoutlabi[1], and Karen Lozano[1],*

[1] *Department of Mechanical Engineering, University of Texas Rio Grande Valley, 1201 West University Drive, Edinburg, TX 78539, USA*

ABSTRACT

α-Fe_2O_3 hollow nanofibers with wall thicknesses of 45 ± 16 nm were fabricated via centrifugal spinning of a solution containing $Fe(NO_3)_3 \cdot 9H_2O$ and polyvinylpyrrolidone. These fibers were subjected to mechanical milling and mixed in ethanol. Polyacrylonitrile (PAN) fiber mats were also fabricated by centrifugal spinning from dimethylformamide-based solutions. The as-prepared PAN fibrous mats were dipped in the iron-oxide suspension. The coated PAN membranes were then subjected to a heat treatment which yielded carbon fibers coated with Fe_3O_4 nanoparticles. Both pure carbon fibers (carbonized PAN fibers) and Fe_3O_4/C composite fibers were used as anode materials in Li-ion batteries. The Fe_3O_4/C composite anode exhibited high specific capacity and good cycle stability when compared to that of the carbon-fiber electrode. An initial discharge capacity (Li insertion) of 882 mAh g^{-1} was obtained for the Fe_3O_4/C composite fibers with promising cycle performance and rate capability. These composite fibers show promising applications as electrode materials in high-performance rechargeable lithium-ion batteries.

Introduction

Carbonaceous materials have been widely used as negative electrodes in lithium-ion batteries (LIBs) due to their high conductivity, low working potential, long cycle life, and low cost [1, 2]. Carbon fibers and nanofibers have recently garnered interest as potential systems to be used in energy-storage devices, including supercapacitors and lithium-ion batteries (LIBs) [3–7]. However, graphite and other carbonaceous materials such as carbon fibers, petroleum

coke, and pyrolytic carbons show low capacities which prevent them from use in high-performance LIBs. Transition metal oxides such as Fe_2O_3, Fe_3O_4, SnO_2, MnO_2, and MoO_2 have shown promising potential as anode materials in LIBs due to their high theoretical capacity [8–11]. However, the volume change in transition metal oxides and other anode materials such as Si and Sn usually results in capacity fading and poor electrochemical performance of the anode after prolonged charge/discharge cycles. Another important factor affecting the electrothermal

Ⓓ Springer

performance of LIB anodes is the formation of the solid electrolyte interface (SEI) layer at the first discharge cycle (Li insertion) [12]. The SEI is a passive layer that tends to block electron flow between electrodes while allowing Li^+ transport between the anode and cathode during the charge/discharge processes [13, 14]. Anode materials including graphite, carbon fibers and Li alloys suffer from a capacity loss at the first charge cycle (Li deinsertion) caused by the decomposition of the liquid electrolyte into various species and further by the formation and instability of the SEI layer [15]. The effect of the SEI layer on the capacity loss in carbon composite fibers and graphene-based anodes with high surface area is more pronounced than that in slurry-based anodes such as thin layers of graphite, Si, Sn and metal oxides coated on copper foil [16, 17]. The morphology and structure of SEI layers in liquid electrolytes have been extensively investigated to better understand the composition and formation mechanism of SEI layers at the anode surface [13, 18].

Organic liquid electrolytes with metal oxide and metallic nanoparticles including Fe_2O_3, Fe_3O_4, SnO_2, silicon (Si) and Sn have been recently used in carbon-fiber matrices to improve the electrochemical performance of carbon composite-fiber anodes in LIBs [8, 19, 20]. Hematite (α-Fe_2O_3) and magnetite (Fe_3O_4) have been extensively studied as potential anode materials for LIBs due to their abundance, low toxicity, and higher theoretical capacities (1004 mAh g^{-1} and 924 mAh g^{-1}, respectively) when compared to the commercial graphite anode (372 mAh g^{-1}) [9, 21, 22].

Given the obtained results, scientists are now seeking facile and scalable methods to fabricate nanocomposite structures of iron oxide for LIB electrodes. For example, results reported on the use of Fe_3O_4 nanocrystals embedded in a mesoporous carbon matrix as an anode in LIBs showed interesting electrochemical performance [21]. The synthesis of the Fe_3O_4/C nanocomposites involved the impregnation of an iron oxide ($Fe(NO_3)_3$) aqueous solution into a pre-formed mesoporous carbon foam (CF) followed by thermal treatment at moderate temperature in an inert atmosphere [21]. Wu et al. [22] reported results on the synthesis of Fe_3O_4 nanocrystals and ordered mesoporous carbon composite by using a wet impregnation method followed by a thermal treatment. The Fe_3O_4/C composite anode delivered a reversible capacity 910 mAh g^{-1} after 50 cycles at 200 mA g^{-1}. Jiang et al. [23] prepared Fe_3O_4/C nanostructures via a modified hydrothermal method. A calcination temperature of 500 °C under argon atmosphere was used to prepare the Fe_3O_4 composites. The Fe_3O_4/CNF composite electrode delivered a reversible capacity of 684 mAh g^{-1} after 55 cycles at 100 mA g^{-1}.

Ma et al. [24] synthesized Fe_3O_4/C nanocomposites using a polyethylene glycol-assisted co-precipitation method. When used as an anode in LIBs, the as-synthesized Fe_3O_4/C nanocomposite structure exhibited a specific discharge capacity of 902.4 mAh g^{-1} after 110 cycles at 1 C corresponding to high-capacity retention at a high current density of 924 mA g^{-1}. The high-capacity retention was attributed to the high Fe_3O_4 nanoparticles loading into the electrode (i.e., 96 wt% Fe_3O_4 content in the Fe_3O_4/C nanocomposites based on the TGA results) [24]. Lang et al. [25] utilized the electrospinning method to fabricate a porous structure of Fe_3O_4/C composite followed by calcination at 500 °C for 2 h. The electrochemical performance of the Fe_3O_4/C microbelt anode was evaluated, where a specific capacity of 710 mAh g^{-1} was obtained after 50 cycles at 0.2 C (i.e., at 184.8 mA g^{-1}). Wang et al. [26] prepared 1D Fe_3O_4/C composite microrods using a precipitation method. The Fe_3O_4/C composite electrode delivered a capacity of 650 mAh g^{-1} after 100 cycles which was much higher than that obtained for Fe_3O_4/C and Fe_3O_4 nanospheres (250 mAh g^{-1} and 165 mAh g^{-1}, respectively).

Fe_3O_4/C composite fibers have been recently synthesized and used as anode materials in LIBs. The results reported in these studies are promising. The Fe_3O_4/C composite fibers were prepared by electrospinning of polymer/iron-oxide precursor solutions and subsequent thermal treatment [27–29] and by anchoring Fe_3O_4/C nanoparticles on nanofiber aerogels from bacterial cellulose [16, 30]. These Fe_3O_4/C composite-fibers anode delivered good capacity retention and improved rate performance [27–30].

Recently, centrifugal spinning has been used as a scalable and high-throughput method to prepare a variety of polymeric, metal oxide, and carbon nanofibers as well as composite materials for use in LIBs [31]. A number of studies have focused on the synthesis of nanofiber-based membranes, while others have specifically focused on the electrochemical performance of these membranes [32–35].

The aim of this work is to synthesize and fabricate Fe_3O_4/carbon composite fibers for use as anode materials in lithium-ion batteries. The purpose of coating PAN fibers with Fe_3O_4 nanoparticles is to improve the electrochemical properties of Fe_3O_4/-carbon composite-fibers anode. To the authors' knowledge, this method has never been used for coating carbon fibers with metal oxide nanoparticles. α-Fe_2O_3 hollow nanofibers were synthesized by centrifugal spinning a solution of polyvinylpyrrolidone and iron nitrate which was subsequently heat treated at 600 °C. PAN nanofiber mats were prepared and coated with the fabricated iron-oxide nanofibers, and the coated PAN membranes were subsequently carbonized at 800 °C for 1 h. The as-synthesized Fe_3O_4/C composite fibers were used as anode materials in rechargeable lithium-ion batteries, and its electrochemical performance was systematically investigated.

Materials and methods

Materials and characterization methods

Polyvinylpyrrolidone (PVP) with an average molecular weight of 1300000 g mol^{-1}, polyacrylonitrile (PAN) with an average molecular weight of 150000 g mol^{-1}, dimethylformamide (DMF), ethanol, 99.5%, and iron nitrate, 99% ($Fe(NO_3)_3 \cdot 9H_2O$) were purchased from Fisher Scientific Co. and used without further modification. The commercial lithium foil, lithium salt (LiPF6), ethylene carbonate (EC), and dimethyl carbonate (DMC) were purchased from MTI corp., USA. A Whatman glass microfiber from GE healthcare was used as the separator.

Scanning electron microscopy (SEM) and energy-dispersive X-ray analysis (EDAX) were performed using a Sigma VP Carl Zeiss. X-ray photoelectron spectrometry (XPS) was conducted using a Thermo Scientific K-α instrument equipped with monochromatized Al Kα radiation (1486.7 eV). For all the tests, a spot size of 400 μm for the X-ray beam was implemented. All the EDAX and XPS tests were conducted along with a reference sample (pristine carbon fiber sample). The quantification analysis was performed at various points, and average ratio is reported. The error bars for EDAX and XPS quantification results were ± < 3% and ± < 2%, respectively. Thermogravimetric analysis (TGA; Q500, TA

Instruments) of Fe_3O_4/C composite fibers was carried out with a heating rate of 3 °C min^{-1} in air. The X-ray diffraction (XRD) patterns were taken from 2θ of 10°–90° with a step of 0.1 using a Bruker D8 Advanced X-ray diffractometer. The electrochemical performance was investigated by carrying out galvanostatic charge–discharge experiments at a current density of 100 mA g^{-1} and between 0.05 and 3.0 V (vs. Li/Li$^+$). The cyclic voltammetry tests were performed by the Bio-Logic BCS-810 with a scan rate of 0.1 mV s^{-1}. The electrochemical performance of the samples was evaluated using coin cells of CR2032 type and assembled in a glove box filled with pure argon gas with oxygen and moisture content < 0.5 ppm. For the lithium-ion cells, lithium metal foil was used as the counter electrode. The electrolyte consisted of 1 M LiPF$_6$ solution in ethylene carbonate (EC)/dimethyl carbonate (DMC) (1:1 v/v), with a Whatman glass microfiber membrane as the separator. The pure carbon fiber samples and Fe_3O_4/C composite electrodes formed flexible free-standing fibers, which were punched directly and used as binder-free electrodes without any additives. The average electrode thickness was about 2 mm, and the average weight was in the range of 3–7 mg.

Fabrication of iron-oxide nanofibers

A solution of PVP and iron nitrate was prepared by using a sol–gel method. PVP (28% w/w) was dissolved in water, mixed, and stirred for 4 h. Then, an aqueous solution of ($Fe(NO_3)_3 \cdot 9H_2O$) (2 g) was prepared and mixed with the PVP solution and set under stirring condition at room temperature for at least 3 h. The PVP/iron nitrate fibers were prepared using the centrifugal spinning method. The solution was spun on a Cyclone instrument (FibeRio Technology Corp.) at rotational speeds in the range of 7000–7500 rpm. Bright-yellow-colored fibrous mats were obtained after spinning the fibers at 27 °C with a relative humidity (R.H.) of 60–65%. To obtain α-Fe_2O_3 hollow nanofibers, the prepared mats were heat treated at a temperature of 600 °C for 1 h under air atmosphere. The resultant iron-oxide nanofibers were saved in sealed plastic bags.

Fabrication of nanocomposite fibers

A solution of PAN (12% w/w) and DMF was prepared and placed under vigorous stirring conditions

for at least 6 h. The solution was then subjected to centrifugal spinning at a rotational speed of 7000–7500 rpm at room temperature with a R.H. of 40–45%. The prepared nonwoven PAN fibrous mat was immersed in a solution of crushed α-Fe_2O_3 nanofibers and ethanol (containing 0.5 w/w% of iron oxide) for at least 3 h (as depicted in Fig. 1). The coated fibrous mat was then taken from the solution and placed in the oven at a temperature of 240 °C for 30 min. Finally, the coated fibrous mat was carbonized at 800 °C (heating rate of 3 °C min^{-1}) under a nitrogen atmosphere for 1 h.
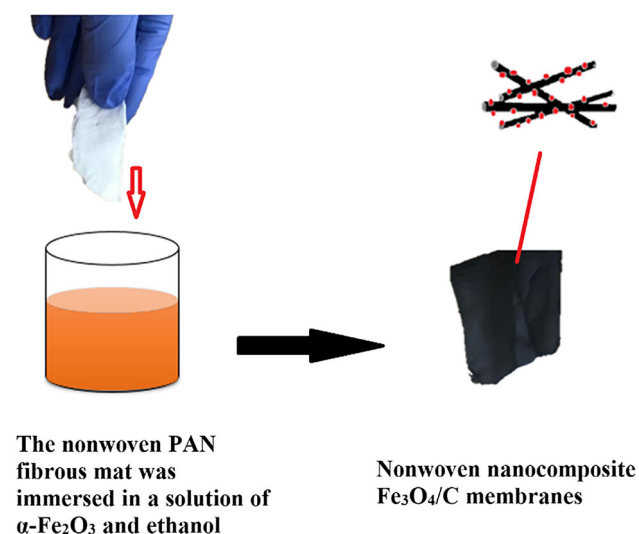
Results and discussion

Figure 2a, b shows SEM images of the resultant iron-oxide hollow fibers after calcination at 600 °C (different magnifications, 1 μm and 200 nm, respectively). It is clearly shown in the figure that the nanofibers are hollow and porous. The size of the pores on the surface of the fibers was found to be 10–125 nm. The fibers show an average diameter of 760 ± 94 nm with wall thicknesses of ca. 45 ± 16 nm. Figure 2c shows the SEM images of the PAN nanofibers; these fibers show an average diameter of 1291 ± 190 nm. Figure 2d shows the SEM micrographs of the Fe_3O_4/C composite fibers; the average fiber diameter was found to be 627 ± 74 nm. As shown in Fig. 2d, the CNFs are decorated with well-dispersed nanosized particles of Fe_3O_4. Figure 2e, f

shows clearly the presence of both iron-oxide nanoparticles and short hollow nanofibers, as depicted in the area with yellow color. The composition of the CNFs and Fe_3O_4/C composite nanofibers was further analyzed by EDAX (Fig. 2g, h). It is observed in the figure that the loaded nanoparticles on the carbon fibers structure reveal the presence of Fe and O elements. The atomic ratios of 62% C, 4% N, 22% O, and 12% Fe were depicted for the selected area (Fig. 2g).

Figure 3a shows the XRD diffraction pattern of the as-synthesized iron-oxide nanofibers. The diffraction peaks appearing at 2θ of 23.84°, 33°, 35.50°, 40.83°, 49.32°, 53.84°, 57.32°, 62.16°, 63.84°, and 71.66° reveal the formation of hematite α-Fe_2O_3 phase of iron oxide. Figure 3b displays the diffraction pattern of the PAN-carbonized fibers and the Fe_3O_4/C composite nanofiber membrane. The diffraction peaks appearing at 2θ values of 18.17°, 30.18°,35.50°, 43°,53.68°, 57°, 62.51° are indexed to (111), (220), (331), (400), (422), (511), and (440) planes and depict the Fe_3O_4 crystalline structure. The broad peak around 24° reflects the graphite structure of pure carbon fibers. The results confirmed the conversion of α-Fe_2O_3 phase to Fe_3O_4 during the carbonization step at 800 °C [36]. XRD analysis of the nanocomposite structure also confirmed the EDAX mapping results which depicted the presence of Fe and O elements for the nanoparticles on the surface of carbon fibers.

TGA tests ran at 3 °C min^{-1} were performed to investigate the thermal decomposition of Fe_3O_4/C composite fibers under air atmosphere. Figure 3c confirms that the degradation of the carbon based matrix in the composite was observed at around 500 °C as indicated by the location of peak in the weight derivative. The Fe_3O_4/C composite fibers underwent a significant weight loss including two main steps upon further increasing temperature. The weight loss occurred below 100 °C was due to the loss of adsorbed water in the composite fibers and the second, above 300 °C, is the result of the degradation process of the carbon phase in the composite indicating that the carbon fibers are in an amorphous phase. This is confirmed by XRD analysis obtained on carbon fibers (Fig. 3b). The TGA results confirm that the amount of Fe_3O_4 in the composite fibers is about 21.5% weight, and this is based on the weight loss of the carbon fibers in the composite indicating weight retention of 21.5% of Fe_3O_4 in the composite fibers.

**Figure 1** Schematics of the fabrication process for the Fe_3O_4/C composite nanofiber membrane.

The nonwoven PAN fibrous mat was immersed in a solution of α-Fe_2O_3 and ethanol

Nonwoven nanocomposite Fe_3O_4/C membranes

Figure 2 a, **b** SEM images of the as-synthesized α-Fe$_2$O$_3$ hollow nanofibers at different magnifications (1 μm and 200 nm), **c** PAN fibers after spinning, not carbonized, **d** composite structure, α-Fe$_2$O$_3$ coated carbon fibers, **e**, **f** iron-oxide hollow nanofibers (some of them identified in the areas with yellow color) before and after carbonization step, **e**, **f** EDAX mapping of the selected area (**g**) which shows the presence of C, N, O, and Fe elements (**h**).
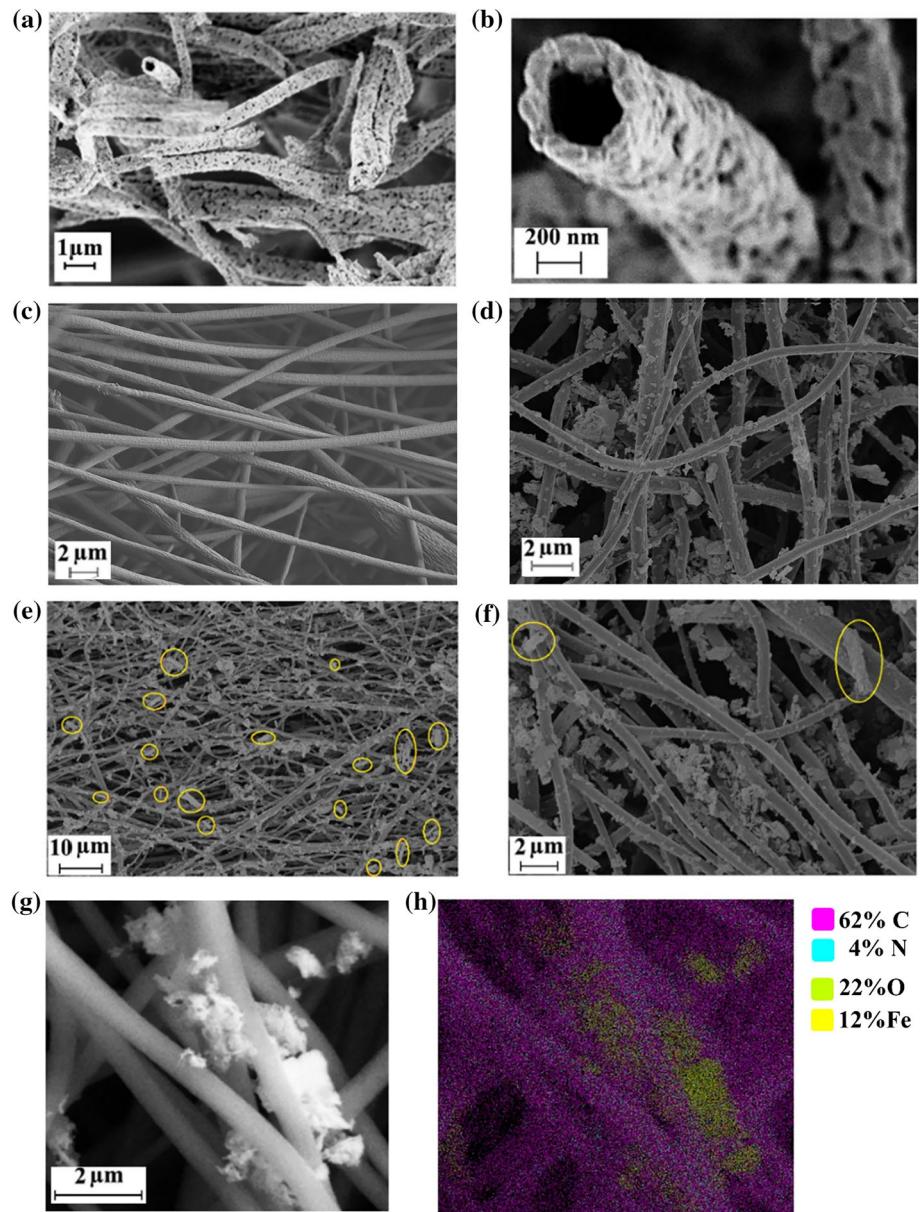
The XPS analysis was conducted for pure carbon fibers and Fe$_3$O$_4$/C composite nanofibers and is presented in Fig. 4. Figure 4a represents the XPS survey spectra for pure carbon fibers and Fe$_3$O$_4$/C composite nanofibers. As illustrated in Table 1, the atomic percentages of C 1s 76.15%, O 1s 3.12%, and N 1s 20.73% were obtained for pure PAN-based carbon fibers compared to C 1s 52.58%, O 1s 28.26%, N 1s 6.07%, and Fe 2p 13.09% for the Fe$_3$O$_4$/C composite nanofibers. The difference between the carbon content of the pure and nanocomposite samples is around 25%, while the ratio of oxygen content in nanocomposite sample compared to the pure carbon

fibers sample is almost 9. The extra oxygen content in the nanocomposite sample can be attributed to the Fe$_3$O$_4$ structure. The deconvolution of Fe 2p peaks, as shown in Fig. 4b, was fitted with two main peaks at 723.8 eV and 711.6 eV and two satellite peaks at 733.2 eV and 717.6 eV, respectively, for 2$p_{3/2}$ and 2$p_{1/2}$. The peak at 723.8 eV is related to Fe 2$p_{3/2}$, and the peak at the binding energy of 711.6 eV is attributed to Fe 2$p_{1/2}$. In other relevant studies, the peak between 710.3 and 711.7 was corresponded to Fe^{III} (octahedral) crystalline structure [37, 38]. Figure 4c shows the XPS spectrum for O 1s peaks which can be fitted to three peaks at binding energy of 530.3, 532,
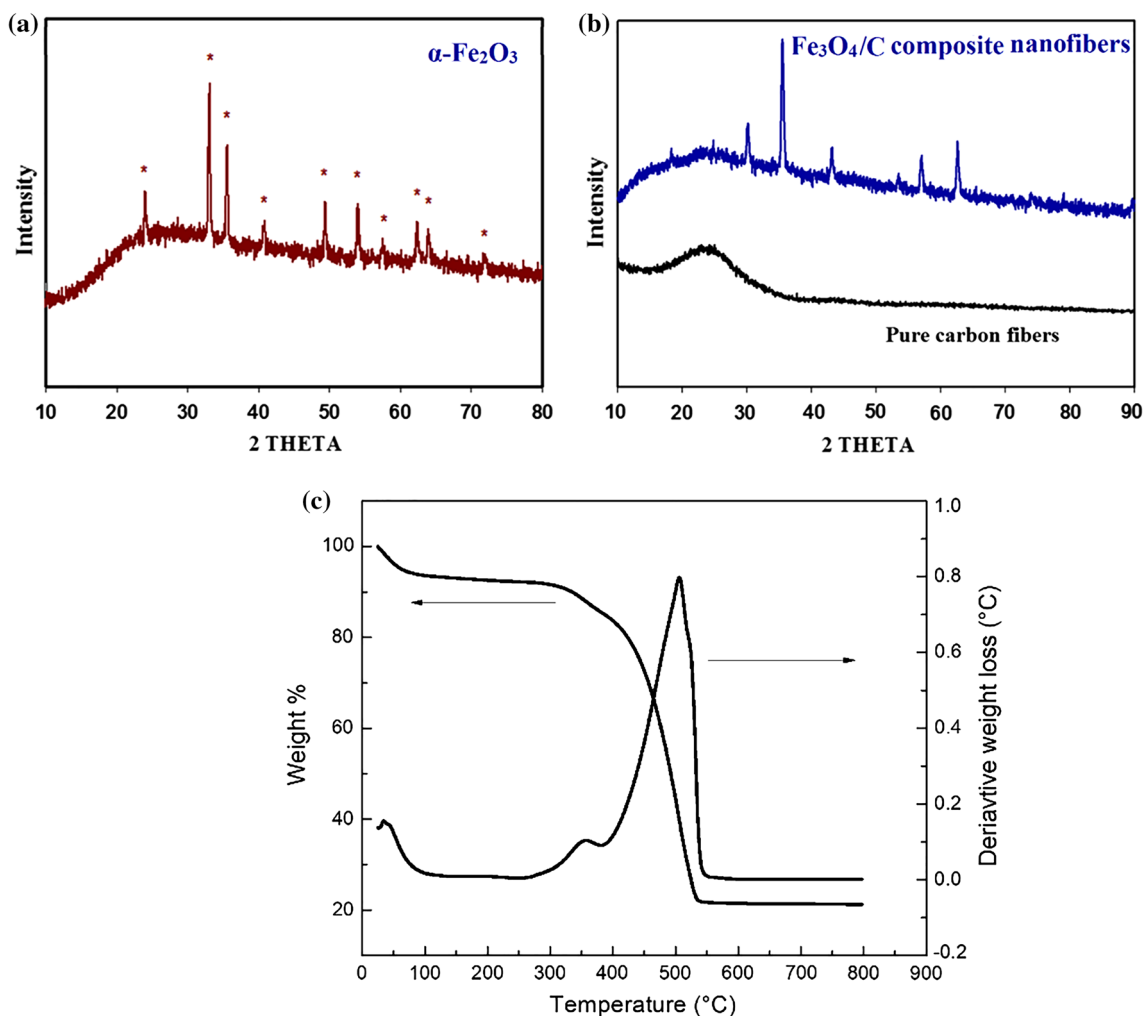
Figure 3 XRD patterns of the fabricated α-Fe$_2$O$_3$ nanofibers (**a**), pure carbon fibers (**b**), and Fe$_3$O$_4$/C composite nanofibers (**b**), thermogravimetric analysis (TGA): TGA curve of the Fe$_3$O$_4$/C composite nanofibers and the first derivative of TGA plot (**c**). The TGA thermogram was conducted in air atmosphere. The sample was heated from 25 to 800 °C at a heating rate of 3 °C min^{-1}.

and 533 eV. The main intense peak at 530.3 eV is attributed to Fe–O which has almost 83% of the whole area. The two small shoulders at $\sim$ 532 eV and $\sim$ 533 eV can be assigned to the surface traps [39] (C=O and O–C=O bands, respectively). The deconvolution of carbon peaks in Fig. 4d exhibits a peak at $\sim$ 284.6 eV with the highest intensity which is corresponded to graphitic carbon. The peak at $\sim$ 286.5 eV is related to a combination of different bonds of C–N, C–O, and C=O [40], and the other peak at a binding energy $\sim$ 288.4 eV can be assigned to carboxyl groups C–C=O.

The lithium storage properties and electrochemical performance of the pure carbon fibers and Fe$_3$O$_4$/C composite fibers were investigated using galvanostatic charge/discharge experiments for 100 cycles at 100 mA g^{-1} and over a voltage window between 0.05 and 3.0 V (vs. Li/Li$^+$). Figure 5a, b shows the charge/discharge curves of the pure carbon fibers and Fe$_3$O$_4$/C nanocomposite fiber anodes, respectively. The initial discharge capacities (Li insertion) of the carbon fibers and nanocomposite fibers are 520 and 882 mAh g^{-1}, respectively, while the initial charge capacities (Li deinsertion) are 200 and 650 mAh g^{-1}, indicating a higher loss in capacity at the first cycle in the carbon fibers compared to the Fe$_3$O$_4$/C nanocomposite. The loss in capacity at the first cycle (irreversible capacity) is mainly due to the SEI formation and also to the high surface area-to-volume ratio of the fibers. The charge–discharge profile of the Fe$_3$O$_4$/C nanocomposite fibers (Fig. 5b) shows a long potential plateau at 0.8 V, which can be
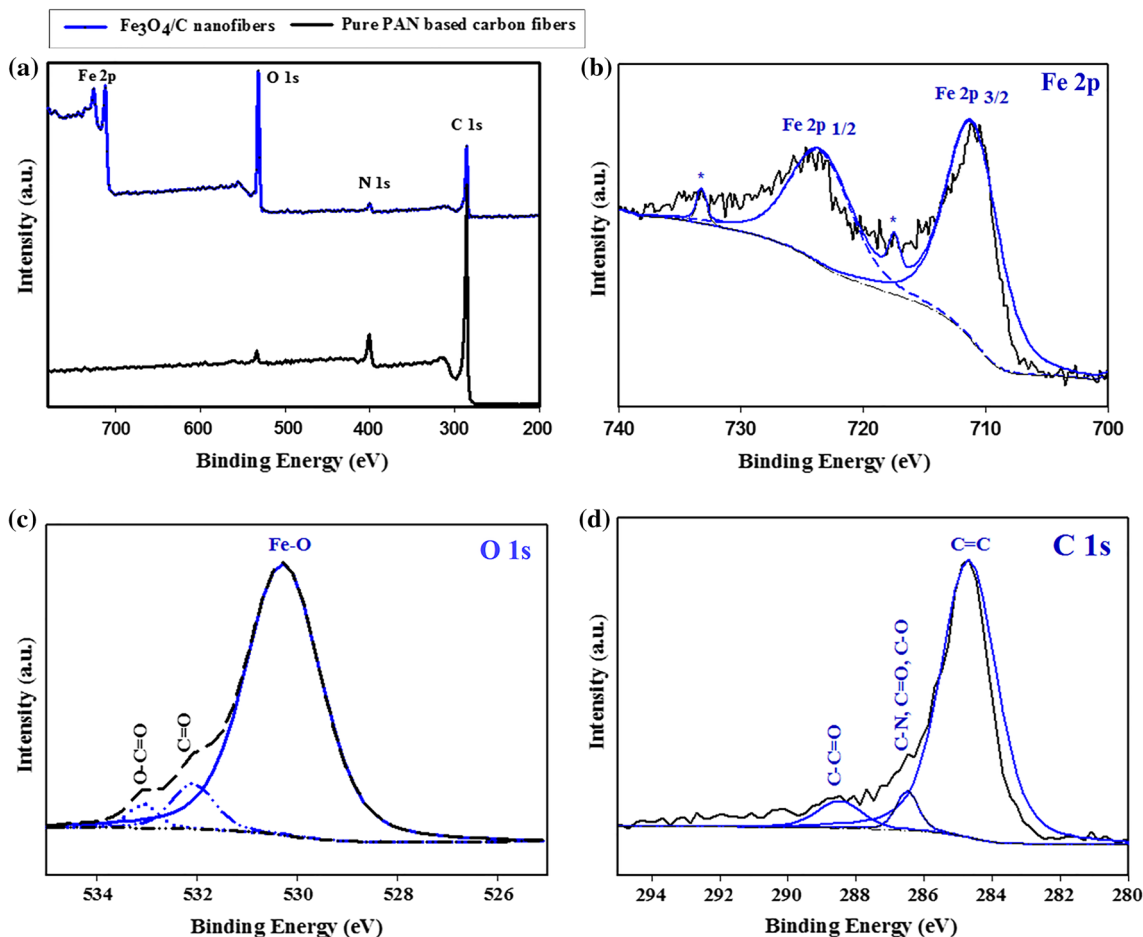
Figure 4 Survey XPS spectra of both pure carbon fibers and the Fe$_3$O$_4$/C composite nanofibers (**a**), deconvoluted spectra of nanocomposite structure for Fe 2p (**b**), O 1s (**c**), and C 1s (**d**).

Table 1 Surface composition of developed carbon fibers and Fe$_3$O$_4$/C composite nanofibers

Surface composition (at%)	C	O	N	Fe
Carbon fibers	76.15	3.12	20.73	0
Fe$_3$O$_4$/C composite nanofibers	52.58	28.26	6.07	13.09

The values were taken from XPS measurements

attributed to the reduction reaction of the oxidation state of iron Fe^0 accompanying the formation of amorphous Li$_2$O simultaneously [22]. The reversible capacity at the second to 100th cycles is stable indicating good capacity retention and Columbic efficiency between 97 and 99%.

Figure 5c, d shows the cycle performance at 100 mA g^{-1} for the carbon fibers and Fe$_3$O$_4$/C composite fibers, respectively. It is obvious that the capacity for both anodes decreases sharply after the

first discharge cycle. The capacity fading at the first cycle is caused by the high irreversible capacity and the formation of the SEI layer within the first cycle, resulting in a Coulombic efficiency of 26.3% and 61.5% at the first cycle for the carbon fibers and the Fe$_3$O$_4$/C composite fibers, respectively. The carbon fiber and Fe$_3$O$_4$/C anodes exhibit negligible capacity loss from the second cycle to 100th cycles and present 200 and 505 mAh g^{-1} at the 100th cycles, respectively. The capacity of the Fe$_3$O$_4$/C composite fibers remains relatively constant upon cycling after the second cycle, while the Coulombic efficiency increases rapidly after the second cycle and holds at about 100% in subsequent cycles. The capacity of the Fe$_3$O$_4$/C nanocomposite fiber anode at 100 mA g^{-1} and after 100 cycles indicates promising results when compared to those reported in the literature for Fe$_3$O$_4$-related nanocomposites [41–44]. The method used in the present work to prepare Fe$_3$O$_4$/C
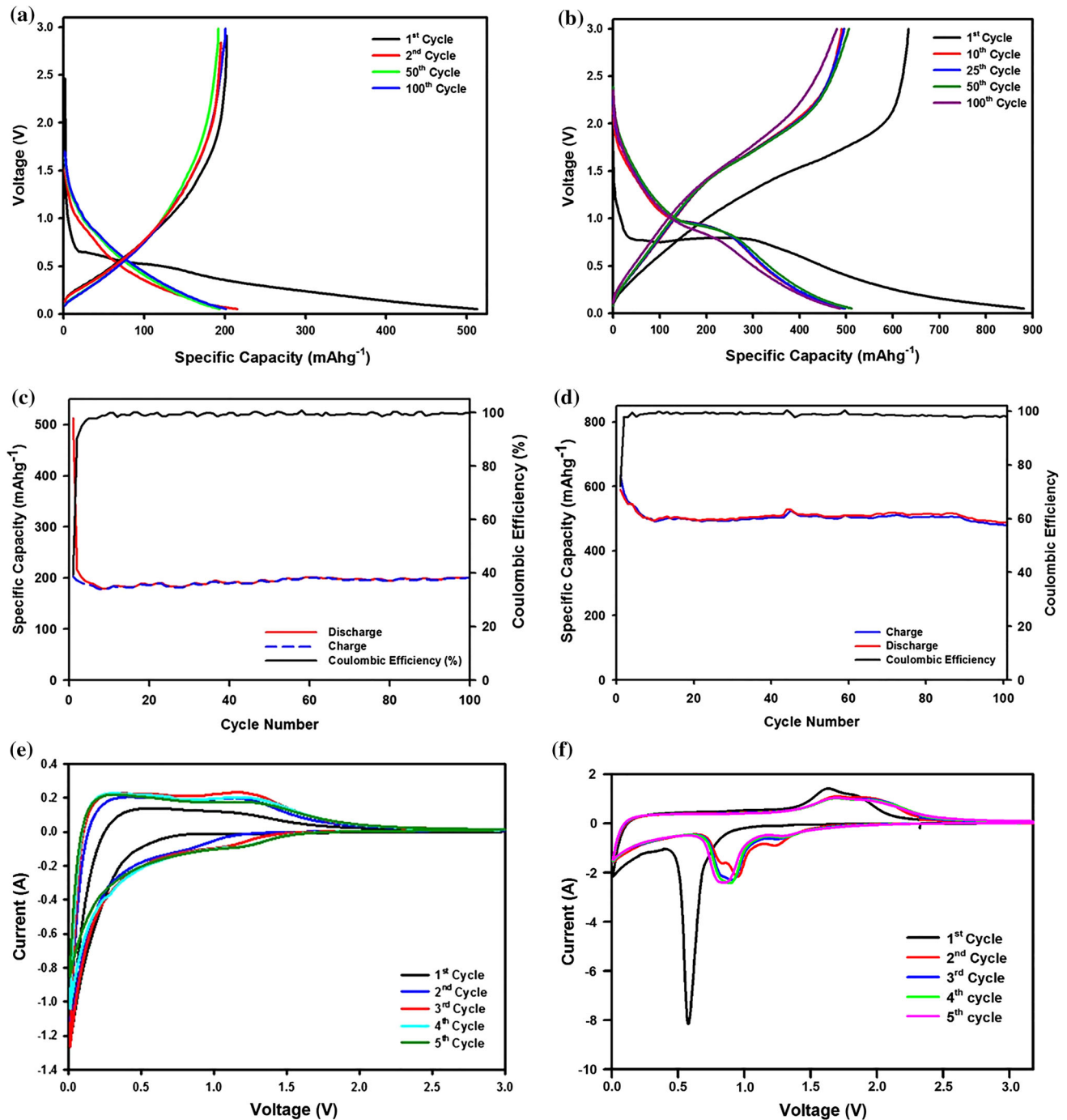
Figure 5 Galvanostatic charge/discharge profiles of pure carbon fibers (**a**) and Fe_3O_4/C composite fibers (**b**) between 1 and 100 cycles, cycle performance of pure carbon fibers (**c**) and Fe_3O_4/C composite fibers (**d**). The experiments were performed at a current density of 100 m Ag^{-1} over a potential window of 0.05–3.0 V. Cycle voltammetry of pure carbon fibers (**d**) and Fe_3O_4/C composite fibers (**c**).

composite fiber anodes shows improved electro-chemical performance and better stability compared to that of pure carbon fiber anodes. To investigate the reaction mechanism of the carbon fiber and Fe_3O_4/C composite fiber anodes, cyclic voltammetry

experiments were performed for the first five cycles at a scan rate of 0.1 mV s^{-1} within the potential window of 3–0.01 V versus Li/Li^+. The results are displayed in Fig. 5e, f. The CV scan for the carbon fiber anode shows two reduction peaks (Li insertion)
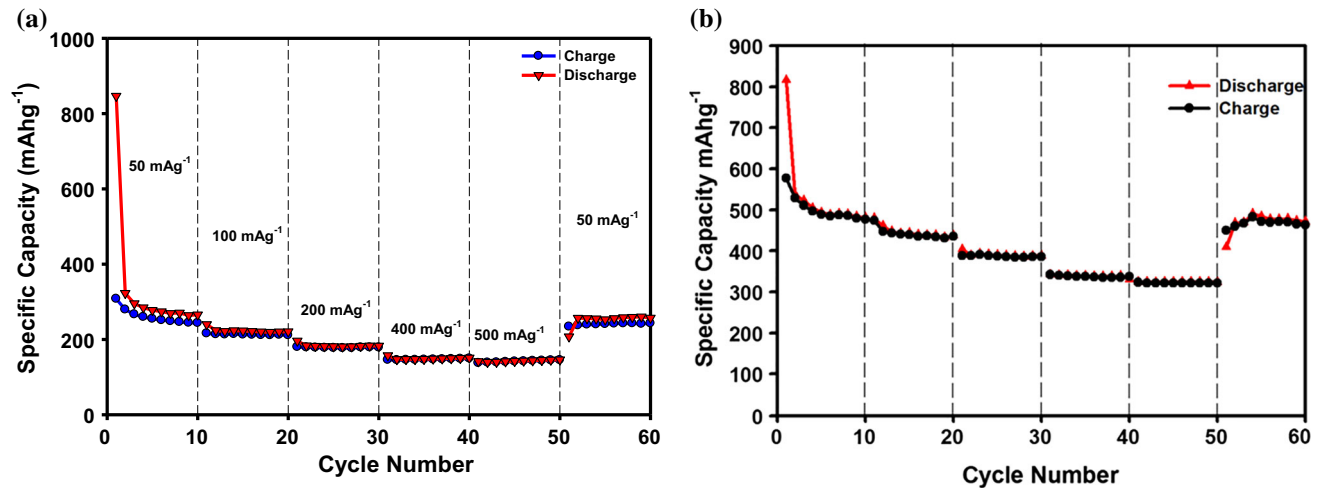
Figure 6 Rate Performance of the carbon fibers (**a**) and Fe_3O_4/C composite-fibers (**b**) anodes at 50, 100, 200, 400, and 500 m Ag^{-1}.

at about 0.3 V and 1.2 V (cathodic scan) during the anodic scan, and two wide oxidation peaks (Li deinsertion) are also observed at about 0.2 and 1.3 V. The small cathodic peak at 0.3 V represents the SEI formation at the first discharge cycle. This shift in potential for the SEI formation might be caused by the thermal treatment of PAN fibers in N_2 atmosphere. Results reported in the literature on the use of carbon fibers in LIBs and sodium-ion batteries indicated that precursor fibers that were carbonized in nitrogen atmosphere or doped with N_2 showed a shift in the SEI potential to lower values [45–47].

As shown in Fig. 5f, at the first cycle, the Fe_3O_4/C composite fibers exhibit a clear cathodic peak at about 0.65 V (reduction reaction). The reduction peak at 0.65 V in the cathodic sweep might be related to the Li insertion into Fe_3O_4 to form $Li_xFe_3O_4$. The voltages for the anodic process (at about 1.7–1.9 V) were much higher than the cathodic ones (0.65 V). This difference in voltage between the reduction and oxidation reactions during the charge/discharge processes was attributed to slow kinetics of the reactions involved in the formation of three components: Fe_3O_4, Fe^0, and Li_2O [21, 48, 49]. The decomposition of $Li_xFe_3O_4$ to form Fe^0 leads to the destruction of the crystal structure and to the formation of the solid electrolyte interface (SEI) layer [9]. Figure 5f shows that the reduction peak at 0.65 V disappears after the first cycle indicating the occurrence of some irreversible processes in Fe_3O_4/C nanocomposite electrode at the first discharge process.

The electrochemical performance of the carbon fiber and Fe_3O_4/C composite nanofiber anodes was further evaluated by conducting current rate (or rate capability tests, rate performance test) experiments of the Li half-cells at different current densities. The anodes were cycled for ten cycles at various current densities of 50, 100, 200, 400, 500 mA g^{-1} and then again at 50 mA g^{-1}, with a cutoff voltage between 0.01 and 3.0 V. This test exemplifies the ability of the anodes to perform at higher current densities as well as evaluate the capacity recovered after being cycled from a high-to-low current density. Figure 6a, b shows the rate performance of the carbon fibers and Fe_3O_4/C nanocomposite fibers, respectively. The irreversible discharge capacities of carbon fibers and Fe_3O_4/C composite fiber electrodes decrease sharply during the initial two cycles at 50 mA g^{-1}; this is caused by the electrolyte decomposition and the SEI formation within the first discharge cycle. The carbon fiber anode shows charge capacities (Li deinsertion) of 259, 207, 173, 143, and 139 mAh g^{-1} at current densities of 50, 100, 200, 400, and 500 mA g^{-1}, respectively. At higher current densities, the rate capability of the carbon fibers anode becomes slower, resulting in lower capacity. The carbon fiber anode shows relatively low charge/discharge capacity rate capability at higher current densities. However, the carbon fibers anode recovers to the original charge capacity of 267 mAh g^{-1} when the current density was restored to 50 mA g^{-1} indicating that the anode shows almost 100% recovery of its capacity. The Fe_3O_4/C nanocomposite electrode (Fig. 6b) exhibits charge capacities (Li deinsertion) of $\sim$ 480, $\sim$ 430,

$\sim$ 390, $\sim$ 335, and $\sim$ 320 mAh g^{-1} at 50, 100, 200, 400, and 500 mA g^{-1}, respectively. The Fe$_3$O$_4$/C composite electrode shows acceptable charge capacities at higher current densities of 400 and 500 mA g^{-1} indicating a rapid reaction process during the Li$^+$ deinsertion cycle. The discharge capacity of the Fe$_3$O$_4$/C composite anode recovered to 480 mAh g^{-1} as the current density was restored to 50 mA g^{-1}, indicating $\sim$ 100% recovery capability and excellent stability at each individual current density.

Conclusions

Hollow nanofibers of α-Fe$_2$O$_3$ with average fiber diameters of 760 $\pm$ 94 nm and wall thickness of ca. 45 $\pm$ 16 were fabricated via a combination of sol–gel and centrifugal spinning followed by calcination at 600 °C. PAN fibers-based membranes were dipped in a solution of α-Fe$_2$O$_3$ and ethanol and subsequently carbonized to develop Fe$_3$O$_4$/C composite fibers. During the carbonization process, the Fe$_2$O$_3$ fibers were reduced to magnetic Fe$_3$O$_4$ fibers. The Fe$_3$O$_4$/C composite fibers and pure carbon fibers (carbonized PAN fibers) were used as binder-free anodes in Li-ion half-cells, where their electrochemical performance was systematically evaluated. The Fe$_3$O$_4$/C composite fibers exhibited good reversible capacity, better cycling stability, and better rate capability when compared to the pristine carbon fibers. The Fe$_3$O$_4$/C composite fibers delivered a higher charge capacity of 505 mAh g^{-1} after 100 cycles at 100 mA g^{-1} compared to 200 mAh g^{-1} for the carbon fibers. The improved electrochemical performance of the Fe$_3$O$_4$/C composite fiber anode is attributed to the high storage capability of the Fe$_3$O$_4$ phase and to the high surface area of the Fe$_3$O$_4$/C nanostructure. The developed Fe$_3$O$_4$/C composite system has promising potential given its low-cost materials and the ability to scale up the process using the centrifugal spinning method.

Acknowledgements

References

[1] Frackowiak E, Beguin F (2001) Carbon materials for the electrochemical storage of energy in capacitors. Carbon 39:937–950

[2] Zhai Y, Dou Y, Zhao D, Fulvio PF, Mayes RT, Dai S (2011) Carbon materials for chemical capacitive energy storage. Adv Mater 23:4828–4850

[3] Ji L, Toprakci O, Alcoutlabi M, Yao Y, Li Y, Zhang S et al (2012) A-Fe$_2$O$_3$ nanoparticle-loaded carbon nanofibers as stable and high-capacity anodes for rechargeable lithium-ion batteries. ACS Appl Mater Interfaces 4:2672–2679

[4] Wang L, Yu J, Dong X, Li X, Xie Y, Chen S et al (2016) Three-dimensional macroporous carbon/Fe$_2$O$_3$-doped porous carbon nanorods for high-performance supercapacitor. ACS Sustain Chem Eng 4:1531–1537

[5] Cho JS, Hong YJ, Kang YC (2015) Design and synthesis of bubble-nanorod-structured Fe$_2$O$_3$–carbon nanofibers as advanced anode material for li-ion batteries. ACS Nano 9:4026–4035

[6] Guan D, Gao Z, Yang W, Wang J, Yuan Y, Wang B et al (2013) Hydrothermal synthesis of carbon nanotube/cubic Fe$_2$O$_3$ nanocomposite for enhanced performance supercapacitor electrode material. Mater Sci Eng B 178:736–743

[7] Mao X, Hatton TA, Rutledge GC (2013) A review of electrospun carbon fibers as electrode materials for energy storage. Curr Org Chem 17:1390–1401

[8] Ji LW, Lin Z, Alcoutlabi M, Zhang XW (2011) Recent developments in nanostructured anode materials for rechargeable lithium-ion batteries. Energy Environ Sci 4:2682–2699

[9] Ji LW, Toprakci O, Alcoutlabi M, Yao YF, Li Y, Zhang S et al (2012) Alpha-Fe$_2$O$_3$ nanoparticle-loaded carbon nanofibers as stable and high-capacity anodes for rechargeable lithium-ion batteries. Acs Appl Mater Interfaces 4:2672–2679

[10] Shi YF, Guo BK, Corr SA, Shi QH, Hu YS, Heier KR et al (2009) Ordered mesoporous metallic moO$_2$ materials with highly reversible lithium storage capacity. Nano Lett 9:4215–4220

[11] Han YT, Wu X, Ma YL, Gong LH, Qu FY, Fan HJ (2011) Porous SnO$_2$ nanowire bundles for photocatalyst and li ion battery applications. CrystEngComm 13:3506–3510

[12] Peled E, Golodnitsky D, Ardel G (1997) Advanced model for solid electrolyte interphase electrodes in liquid and polymer electrolytes. J Electrochem Soc 144:L208–L210

[13] Bhattacharya S, Alpas AT (2012) Micromechanisms of solid electrolyte interphase formation on electrochemically cycled graphite electrodes in lithium-ion cells. Carbon 50:5359–5371

[14] Krueger S, Kloepsch R, Li J, Nowak S, Passerini S, Winter M (2013) How do reactions at the anode/electrolyte interface determine the cathode performance in lithium-ion batteries? J Electrochem Soc 160:A542–A548

[15] Nie MY, Abraham DP, Chen YJ, Bose A, Lucht BL (2013) Silicon solid electrolyte interphase (sei) of lithium ion battery characterized by microscopy and spectroscopy. J Phys Chem C 117:13403–13412

[16] Wan YZ, Yang ZW, Xiong GY, Luo HL (2015) A general strategy of decorating 3d carbon nanofiber aerogels derived from bacterial cellulose with nano-Fe_3O_4 for high-performance flexible and binder-free lithium-ion battery anodes. J Mater Chem A 3:15386–15393

[17] Xing BL, Zeng HH, Huang GX, Zhang CX, Yuan RF, Cao YJ et al (2019) Porous graphene prepared from anthracite as high performance anode materials for lithium-ion battery applications. J Alloys Compd 779:202–211

[18] Nie MY, Chalasani D, Abraham DP, Chen YJ, Bose A, Lucht BL (2013) Lithium ion battery graphite solid electrolyte interphase revealed by microscopy and spectroscopy. J Phys Chem C 117:1257–1267

[19] Zhou G, Wang D-W, Li F, Zhang L, Li N, Wu Z-S et al (2010) Graphene-wrapped Fe3O4 anode material with improved reversible capacity and cyclic stability for lithium ion batteries. Chem Mater 22:5306–5313

[20] Wakihara M (2001) Recent developments in lithium ion batteries. Mater Sci Eng R Rep 33:109–134

[21] Yoon T, Chae C, Sun YK, Zhao X, Kung HH, Lee JK (2011) Bottom-up in situ formation of Fe3O4 nanocrystals in a porous carbon foam for lithium-ion battery anodes. J Mater Chem 21:17325–17330

[22] Wu F, Huang R, Mu DB, Shen XY, Wu BR (2014) A novel composite with highly dispersed Fe3O4 nanocrystals on ordered mesoporous carbon as an anode for lithium ion batteries. J Alloys Compd 585:783–789

[23] Jiang F, Zhao S, Guo J, Su Q, Zhang J, Du G (2015) Fe_3o_4 nanoparticles-wrapped carbon nanofibers as high-performance anode for lithium-ion battery. J Nanopart Res 17:348

[24] Ma YC, Huang YD, Wang XC, Jia DZ, Tang XC (2014) One-pot synthesis of Fe_3O_4/C nanocomposites by peg-assisted co-precipitation as anode materials for high-rate lithium-ion batteries. J Nanopart Res 16:2614

[25] Lang L, Xu Z (2013) In situ synthesis of porous Fe3O4/C microbelts and their enhanced electrochemical performance for lithium-ion batteries. ACS Appl Mater Interfaces 5:1698–1703

[26] Wang Y, Zhang L, Gao X, Mao L, Hu Y, Lou XW (2014) One-pot magnetic field induced formation of Fe3O4/C composite microrods with enhanced lithium storage capability. Small 10:2815–2819

[27] Xu ZL, Zhang BA, Gang Y, Cao K, Garakani MA, Abouali S et al (2015) In-situ tem examination and exceptional long-term cyclic stability of ultrafine Fe3O4 nanocrystal/carbon nanofiber composite electrodes. Energy Storage Mater 1:25–34

[28] Qin XY, Zhang HR, Wu JX, Chu XD, He YB, Han CP et al (2015) Fe_3O_4 nanoparticles encapsulated in electrospun porous carbon fibers with a compact shell as high-performance anode for lithium ion batteries. Carbon 87:347–356

[29] Wu QH, Zhao RF, Zhang X, Li WL, Xu RH, Diao GW et al (2017) Synthesis of flexible Fe3O4/C nanofibers with buffering volume expansion performance and their application in lithium-ion batteries. J Power Sources 359:7–16

[30] Wan YZ, Yang ZW, Xiong GY, Guo RS, Liu Z, Luo HL (2015) Anchoring Fe3O4 nanoparticles on three-dimensional carbon nanofibers toward flexible high-performance anodes for lithium-ion batteries. J Power Sources 294:414–419

[31] Sarkar K, Gomez C, Zambrano S, Ramirez M, de Hoyos E, Vasquez H et al (2010) Electrospinning to forcespinning™. Mater Today 13:12–14

[32] Akia M, Capitanachi D, Martinez M, Hernandez C, de Santiago H, Mao Y et al (2018) Development and optimization of alumina fine fibers utilizing a centrifugal spinning process. Microporous Mesoporous Mater 262:175–181

[33] Weng B, Xu F, Alcoutlabi M, Mao Y, Lozano K (2015) Fibrous cellulose membrane mass produced via forcespinning® for lithium-ion battery separators. Cellulose 22:1311–1320

[34] Zuniga L, Agubra V, Flores D, Campos H, Villareal J, Alcoutlabi M (2016) Multichannel hollow structure for improved electrochemical performance of TiO_2/carbon composite nanofibers as anodes for lithium ion batteries. J Alloys Compd 686:733–743

[35] Agubra VA, De la Garza D, Gallegos L, Alcoutlabi M (2016) ForceSpinning of polyacrylonitrile for mass production of lithium-ion battery separators. J Appl Polym Sci 133:42847

[36] Wu Q, Zhao R, Zhang X, Li W, Xu R, Diao G et al (2017) Synthesis of flexible Fe3O4/C nanofibers with buffering volume expansion performance and their application in lithium-ion batteries. J Power Sources 359:7–16

[37] Poulin S, Franca R, Moreau-Bélanger L, Sacher E (2010) Confirmation of x-ray photoelectron spectroscopy peak attributions of nanoparticulate iron oxides, using symmetric peak component line shapes. J Phys Chem C 114:10711–10718

[38] Poulin S, França R, Moreau-Bélanger L, Sacher E (2010) Confirmation of x-ray photoelectron spectroscopy peak attributions of nanoparticulate iron oxides, using symmetric

peak component line shapes. J Phys Chem C 24:10711–10718

[39] Zhang D, Liu Z, Han S, Li C, Lei B, Stewart MP et al (2004) Magnetite (Fe3O4) core–shell nanowires: synthesis and magnetoresistance. Nano Lett 4:2151–2155

[40] Wilson D, Langell M (2014) Xps analysis of oleylamine/oleic acid capped Fe3O4 nanoparticles as a function of temperature. Appl Surf Sci 303:6–13

[41] Dong YC, Hu MJ, Ma RG, Cheng H, Yang SL, Li YY et al (2013) Evaporation-induced synthesis of carbon-supported Fe3O4 nanocomposites as anode material for lithium-ion batteries. CrystEngComm 15:1324–1331

[42] Liu J, Zhou YC, Liu F, Liu CP, Wang JB, Pan Y et al (2012) One-pot synthesis of mesoporous interconnected carbon-encapsulated Fe3O4 nanospheres as superior anodes for li-ion batteries. Rsc Adv 2:2262–2265

[43] Lang LM, Xu Z (2013) In situ synthesis of porous Fe3O4/C microbelts and their enhanced electrochemical performance for lithium-ion batteries. Acs Appl Mater Interfaces 5:1698–1703

[44] Howard CJA, Carolina V, Parsons JG, Mataz A (2018) The use of Fe$_3$O$_4$/carbon composite fibers as anode materials in lithium ion batteries. MOJ Poly Sci 2:44–46

[45] Zeng LC, Li WH, Cheng JX, Wang JQ, Liu XW, Yu Y (2014) N-doped porous hollow carbon nanofibers fabricated using electrospun polymer templates and their sodium storage properties. Rsc Adv 4:16920–16927

[46] Chen C, Lu Y, Ge YQ, Zhu JD, Jiang H, Li YQ et al (2016) Synthesis of nitrogen-doped electrospun carbon nanofibers as anode material for high-performance sodium-ion batteries. Energy Technol-Ger 4:1440–1449

[47] Qie L, Chen WM, Wang ZH, Shao QG, Li X, Yuan LX et al (2012) Nitrogen-doped porous carbon nanofiber webs as anodes for lithium ion batteries with a superhigh capacity and rate capability. Adv Mater 24:2047–2050

[48] Huang XD, Zhou XF, Qian K, Zhao DY, Liu ZP, Yu CZ (2012) A magnetite nanocrystal/graphene composite as high performance anode for lithium-ion batteries. J Alloys Compd 514:76–80

[49] Poizot P, Laruelle S, Grugeon S, Dupont L, Tarascon JM (2000) Nano-sized transition-metaloxides as negative-electrode materials for lithium-ion batteries. Nature 407:496–499